

Tailoring the near-Surface Composition Profiles of Pressure-Sensitive Adhesive Films and the Resulting Mechanical Properties

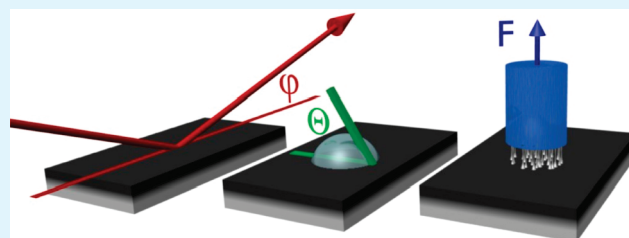
Alexander Diethert,[†] Katharina Ecker,[†] Yana Peykova,[‡] Norbert Willenbacher,[‡] and Peter Müller-Buschbaum^{*,†}

[†]Technische Universität München, Physik-Department E13, Lehrstuhl für Funktionelle Materialien, James-Frank-Strasse 1, 85747 Garching (Germany)

[‡]Institut für Mechanische Verfahrenstechnik und Mechanik, Karlsruher Institut für Technologie (KIT), Kaiserstrasse 12, 76131 Karlsruhe (Germany)

ABSTRACT: We present a possibility of tailoring the near-surface composition profiles of pressure sensitive adhesive (PSA) films by an exposure to atmospheres of different relative humidities (RHs). The statistical copolymer P(EHA-stat-20MMA) with a majority of ethylhexylacrylate (EHA) and a minority of methylmethacrylate (MMA), being cast from a toluene based solution, is chosen as a model system. The near-surface composition profile is probed with X-ray reflectivity. All probed samples show an enrichment of PMMA at the sample surface; however, the near-surface PMMA content strongly increases with increasing RH. The influence of the RH on the composition profile is present down to a depth of 50 nm. Therefore the surface tensions being derived from contact angle measurements do not show any measurable humidity dependence. In contrast, in a mechanical tack test with a smooth punch surface, a strong influence is probed. This observation can be explained by considering the integrated PMMA content over an appropriate near-surface region and the resulting impact on the cavitation process.

KEYWORDS: pressure-sensitive adhesive, solution casting, X-ray reflectivity, surface enrichment



1. INTRODUCTION

Pressure-sensitive adhesives (PSAs) mark one class of adhesives that have the ability to create releasable bonds. PSAs have a wide-spread range of different applications, which includes stick-on notes, adhesive foils, scotch tapes, labels, and reusable packages. Thus PSAs offer the opportunity to connect extremely different materials such as paper, metals, glasses, ceramics, and polymers in a reusable way. Typically, the adhesion is well balanced by the constituents of the PSA film. For example, to install low-tack materials a nontacky component is added in order to limit the contact area between the PSA system and the bonded surface. These added components can be inorganic solid particles like glass beads, calcium carbonate or glassy polymers.¹

For some applications, it is desirable to have a controllable adhesive bond via an external stimulus. One approach is based on the use of a switchable adherent. For example, the adhesion between a switchable polystyrene/poly(2-vinylpyridine) brush and an elastomeric adhesive can be controlled by the use of selective solvents.² With this method, the authors varied the surface composition of the brush and observed a change in the strength of the adhesive bond. The same concept also works when the brush itself is switched from a sticky to a nonsticky state.^{3,4}

Besides the response to selective solvents, the nature of possible stimuli can be very different. Among others, responses of adhesives have been reported to temperature,^{5–7} exposure to light,⁸ presence of water⁹ or water vapor,^{10,11} and the application of an electrical voltage.¹²

Moreover, the performance of an adhesive can also be changed mechanically. Inspired by gecko feet, it is possible to achieve a much stronger shear adhesion force as compared to the normal adhesion force by making use of aligned carbon nanotubes.^{13,14} An alternative approach is a fibrillar structure that is terminated by a continuous film.¹⁵ As long as the system is in a stretched state an enhanced adhesion is measured. When it is mechanically switched to a collapsed state, the adhesion is reduced. Furthermore, Feng and co-workers demonstrated transfer printing based on kinetically switchable adhesion to an elastomeric stamp.¹⁶ Whether a film is deposited on a substrate or picked up by the stamp is determined by the speed of the film/stamp interface.

Most common is the use of temperature as a stimulus to change the adhesion due to a change in morphology of the adhesive in order to achieve a change in tackiness. For example, liquid crystalline polymers can be used because of the big impact of the orientation of the side chains. The transition from a smectic layering toward an isotropic state, within a narrow temperature range, leads to a significant change in tack force.^{17,18} Alternatively, in semicrystalline polymers the adhesive performance can be switched by heating the sample above the melting temperature of the crystals. For this purpose, for example Agirre and co-workers produced waterborne

Received: March 1, 2011

Accepted: May 23, 2011

Published: May 23, 2011

PSAs copolymerized out of ethylhexylacrylate, methacrylic acid and stearyl acrylate.¹⁹ The crystallinity was controlled by the monomer ratio in the formulation, the process conditions and the blending ratio. Because of the change in temperature, the crystallinity was changed, and as a consequence, the shear resistance and the peel strength were altered.

In our investigation, we focus on a stimulus given by the presence of water vapor. In contrast to the simple absence or presence of water vapor, we use different relative humidities (RHs). Our idea is to tailor the near-surface morphology of the adhesive via the RH of the surrounding atmosphere. An increased RH leads to an increased selectivity with respect to the more polar component in the adhesive. To make this effect applicable for adhesives, we use a system that comprises components that differ in polarity and tackiness. The mechanical properties change as a consequence of the altered near-surface composition. Moreover, in a rephrased way, our experiments also contribute to the question what happens when such an adhesive film is stored under different RH conditions.

In literature, the influence of the RH on the morphology of polymers was investigated experimentally for different non-tacky systems. One example is the tuning of the phase separation morphology by selecting the appropriate RH.²⁰ With this approach, in block copolymer electrolytes, the order–disorder transition was affected,²¹ and in polymer blends on prepatterned substrates, the demixing was controlled.²²

Moreover, computer simulations by Klos et al. showed that the RH determines the near-surface composition.²³ In the simulation the composition profile of a two component statistical copolymer P(A-stat-B) near a selective surface was modeled using the bond fluctuation method. With increasing the interaction parameter between the surface and species A, more A-monomers adsorbed near the interface. Underneath this surface enrichment layer, the authors predicted an enrichment of monomers of type B. Stimulated by this simulations, we select a model system based on a statistical copolymer P(A-stat-B), with two blocks A and B. One block is selected to be rigid and the other one tacky as commonly being used in adhesives. To allow for tunability via RH, the blocks of the statistical copolymer differ in polarity. Our model system is the statistical copolymer P(EHA-stat-20MMA) with a composition ratio of 80% of ethylhexylacrylate (EHA) and 20% methylmethacrylate (MMA).

To understand the observed changes in the tack as a function of RH, we determine the corresponding near-surface composition profiles. Recently, we have shown that X-ray reflectivity (XRR) is a well suited method to probe such near-surface composition profiles in adhesive films.²⁴ Moreover, we were able to demonstrate that the near-surface composition influences the tackiness of the adhesive film. We related the adhesive performance of statistical copolymer films composed of 90% EHA and 10% of a glassy monomer to the installed near-surface composition profiles. With decreasing amount of glassy component in a near-surface region, which has a thickness equal to the punch roughness of the tack tester, the tackiness also dropped. The influence of the glassy component on the cavitation process causes such reduced tack.²⁵

In addition to the determination of the near-surface composition and tack as a function of RH, we analyze the dependence of the surface tension of our PSA model system²⁶ P(EHA-stat-20MMA).

This article has the following structure: After a description of the investigated samples and a brief introduction in the main experimental methods XRR, contact angle measurement and

mechanical tack test, the resulting composition profiles as well as their impact on the surface tension and the tackiness are presented and discussed. The article concludes with a summary of the results and a short outlook.

2. EXPERIMENTAL SECTION

2.1. Sample Preparation. The statistical copolymer P(EHA-stat-20MMA) with a monomer composition of 80% ethylhexylacrylate (EHA) and 20% methylmethacrylate (MMA) and a molecular weight of $M_w = 248$ k is chosen for this investigation. P(EHA-stat-20MMA) was polymerized with a radical solution polymerization technique and, thus, shows a broad molecular weight distribution, which is typical for adhesive applications.

For the film preparation the polymer was dissolved in toluene using a concentration of 94.5 g/L. Microscope slides (MENZEL, 76 mm × 26 mm × 1 mm), which had been flushed with compressed, oil-free nitrogen directly before casting the solution in order to remove dust particles, are used as a substrate. With the chosen solution concentration, the desired film thickness of 50 μm is achieved by casting a solution volume of 1 mL onto the substrate. Weight measurements have been carried out to confirm the thickness. The advantage of such thick films is that, because of their short-ranged nature,^{27–29} the interactions between the substrate and the near-surface region can be neglected and thus, a maximum sensitivity to the RH is achieved. The complete preparation process is performed under a constant temperature of 20 °C which is kept constant by air-conditioning.

Because the composition profiles are very sensitive to the evaporation speed being closely related to the accessible volume for the evaporating solvent and thus to the size and shape of the sample chamber, as well as the humidity and the temperature, the sample preparation is done in two steps. In a first step, the casting of the liquid is performed in a desiccator (flange diameter 118.5 mm, SCHOTT, DURAN) filled with silica gel which produces a RH that is measured to be lower than 2%. The substrate is carefully aligned beforehand to ensure a uniform film thickness. The drying time at such low humidity is 24 h. As a consequence, a well-defined and reproducible film structure is established.

In a second step, the dried sample is placed into a humid environment, which is provided by another desiccator filled with saturated salt solution. To reduce unnecessary exposure to ambient air and thus uncontrolled conditions, the sample stage in the second desiccator is already prealigned and the lid is closed immediately after placing the sample. The storage time in the second desiccator is another 24 h, giving again rise to a well-defined and reproducible film structure.

In summary, with the chosen preparation procedure the observed composition profiles only depend on the installed humidity. If the solution had been casted directly under humid conditions, it would have been impossible to separate the effect of interface selectivity due to humidity from a decelerated evaporation speed due to a reduced evaporation volume originating from the presence of water vapor in the desiccator.

The corresponding X-ray reflectivity, contact angle and probe tack measurements were performed immediately after removing the sample from the desiccator. Conformational changes of the sample until the end of the experiments are not to be expected because the time scale for significant molecular reorganization is on the order of days.²⁴

Six different RHs are selected, whereas one sample is kept in the desiccator filled with silica gel for the entire 48 h and, thus represents the preparation under dry conditions. The five higher RHs are (23.11 ± 0.25)%, (43.16 ± 0.33)%, (54.38 ± 0.23)%, (75.47 ± 0.14)% and (85.11 ± 0.29)% provided by saturated water-based solutions of potassium acetate, potassium carbonate, magnesium nitrate, sodium chloride and potassium chloride, respectively.³⁰

2.2. X-ray Reflectivity (XRR). The X-ray reflectivity (XRR) experiments were performed with a “Siemens D5000 Diffraktometer”. The width of the beam was chosen to be 12 mm and the wavelength was

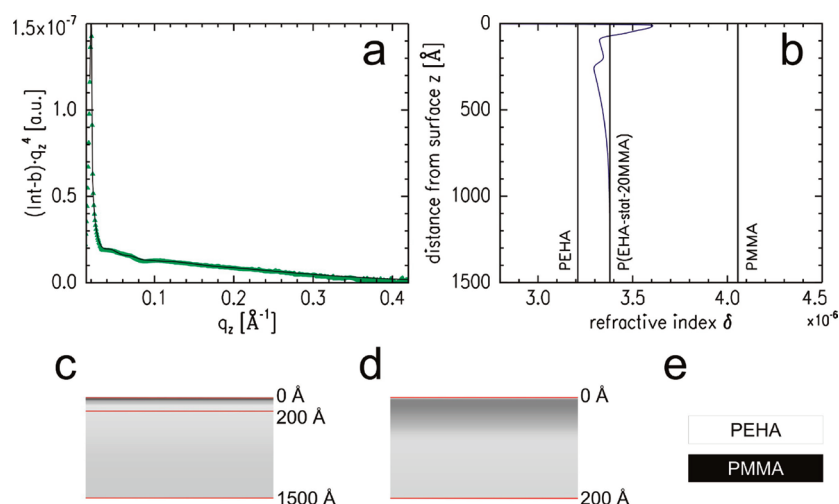


Figure 1. (a) Measured XRR data (symbols) in Fresnel-normalized representation of a P(EHA-stat-20MMA) film casted and dried in a desiccator for 24 h and respective fit to the data (solid line). (b) Corresponding refractive index profile to the shown fit. The vertical lines mark the values of the refractive indices of P(EHA-stat-20MMA) and the related homopolymers as shown by the labels. (c) Black and white coded composition profile calculated from the refractive index profile. The horizontal lines mark the positions $z = 0, 200,$ and 1500 \AA , measured from the sample surface. (d) Zoom into the near-surface region of the composition profile. (e) Color code used in the composition profiles.

$\lambda = 1.54 \text{ \AA}$ corresponding to the Cu– K_{α} line. For beam collimation a slit system was used in combination with a tantalum knife edge. The reflected beam was detected with a scintillation counter in front of which a graphite monochromator was situated to filter the Cu– K_{β} line. For small reflection angles an absorber reducing the intensity by a factor of approximately 100 is used to avoid detector saturation and thus wrong counting rates.

For an incident angle φ , the detector was positioned at an angle 2φ measured with respect to the incoming beam. The reflectivity curves cover an angular range of $0^{\circ} < 2\varphi < 7^{\circ}$ with a maximum resolution of 0.01° . To account for the lower counting rates at higher incident angles, this range is divided into three overlapping intervals with adjusted measurement times which were merged according to the selected integration times.

For a pronounced representation of the features in the measured XRR curves we plot $(I(q_z) - b)q_z^4$ as a function of the scattering vector $q_z = 4\pi\sin(\varphi)/\lambda$. In this so-called Fresnel-normalized representation $I(q_z)$ is the reflected intensity which is normalized to 1 and b is the background which is assumed to be constant. The XRR data analysis was performed with the reflectivity simulation and analysis tool Parratt32.³¹ From a fit to the data using the Parratt algorithm³² the refractive index profile $\delta(z)$ is obtained. $\delta(z)$ is the real part of the complex refractive index $n(z) = 1 - \delta(z) + i\beta(z)$ and z is the distance from the sample surface.

The δ -values for the involved homopolymers related to the statistical copolymer P(EHA-stat-20MMA) are $\delta(\text{PEHA}) = 3.21 \times 10^{-6}$ and $\delta(\text{PMMA}) = 4.06 \times 10^{-6}$. They are calculated via the mass density of the homopolymers, the number of electrons of the respective monomers and the corresponding dispersion correction factors in dipole approximation of the atom form factor.^{33,34} The high contrast between $\delta(\text{PEHA})$ and $\delta(\text{PMMA})$ makes it easy to distinguish between the two components. The average refractive index of the statistical copolymer is calculated by weighting the refractive indices of the respective homopolymers by their composition ratio: $\delta(\text{P(EHA-stat-20MMA)}) = 3.37 \times 10^{-6}$.

2.3. Contact Angle Measurements. The contact angle measurements were carried out on a “dataphysics contact angle system OCA” at a temperature of $20 \text{ }^{\circ}\text{C}$, which was kept constant by air-conditioning. A sessile droplet with a volume of $2 \mu\text{L}$ was dispensed by a computer controlled syringe and brought in contact with the surface of the adhesive film under investigation by a movable sample stage.

Immediately after the droplet was placed onto the sample, the stage was moved into the focus of a prealigned camera with high magnification and a movie of the droplet was recorded for around 70 s with a frame rate of 15 images per second.

The contact angle θ of the droplet with respect to the sample was extracted with the “dataphysics SCA20” software from each image of the movie by fitting an ellipsoidal contour to the droplet shape. The influence of gravity on the droplet shape can be neglected for such small volumes justifying the assumption of an ellipsoidal shape.³⁵ As a result, θ is determined as a function of time t and the equilibrium contact angle θ_f is obtained from a fit to these curves.

The resulting surface energy was determined by the method of Owens and Wendt.³⁶ For this purpose, the experiment was performed with six different test liquids. The corresponding dispersive (index d) and polar (index p) components of the surface tension of the used liquids³⁷ are $\gamma_d(\text{paraffin oil}) = 29.5 \text{ mN/m}$, $\gamma_p(\text{paraffin oil}) = 0 \text{ mN/m}$, $\gamma_d(\text{diiodomethane}) = 47.4 \text{ mN/m}$, $\gamma_p(\text{diiodomethane}) = 2.6 \text{ mN/m}$, $\gamma_d(\text{ethylene glycol}) = 29.0 \text{ mN/m}$, $\gamma_p(\text{ethylene glycol}) = 19.0 \text{ mN/m}$, $\gamma_d(\text{formamide}) = 23.5 \text{ mN/m}$, $\gamma_p(\text{formamide}) = 33.4 \text{ mN/m}$, $\gamma_d(\text{glycerol}) = 21.2 \text{ mN/m}$, $\gamma_p(\text{glycerol}) = 41.5 \text{ mN/m}$, $\gamma_d(\text{water}) = 19.9 \text{ mN/m}$, $\gamma_p(\text{water}) = 52.2 \text{ mN/m}$. At least seven data sets $\theta(t)$ were recorded for each sample to reduce the statistical error.

2.4. Mechanical Tack Test. For the probe tack tests²⁵ two different setups were used. Both were operated under room temperature conditions. One is a custom-designed apparatus equipped with a “FGP XF-3030” force sensor and a probe made of stainless steel. The other device is a “Stable Micro System” texture analyzer “TA.XT” using a “Kistler” quartz force sensor and a silicon punch to contact the adhesive. Both probes are flat-ended and have cylindrical shape. The contact areas of both punches were highly polished to almost the same roughness values of $R_a = 17 \text{ \AA}$ for stainless steel and $R_a = 16 \text{ \AA}$ for silicon, respectively. These values were determined by atomic force microscopy measurements.

At least 8 repetitions of the tack test were performed per sample so that the given values of the maximum stress as well as the tack energy represent an average with sufficient statistical significance. The position on the sample was changed after each measurement to ensure that each time a fresh spot with an untouched PSA surface was provided. Between two subsequent measurements the punch was carefully cleaned with a

soft tissue soaked with toluene so that possible PSA residues or dust particles were removed. Additionally, to monitor the cavitation process, the contact area was filmed with a CCD camera. Moreover, the optical control was used for the alignment of the punch with respect to the PSA surface.

For all investigated samples, the punch approached and contacted the sample at a velocity of 0.1 mm/s. The movement stopped instantaneously after a contact pressure of 0.32 MPa had been reached. After a waiting time of precisely 10 s during which no further movements were performed, the punch was retracted with a speed of again 0.1 mm/s and the force and the distance were measured simultaneously. Finally, the stress was calculated as the measured force divided by the punch area and the strain as the punch distance from the point of zero stress divided by the film thickness.

2.5. Optical Microscopy. Before the XRR experiments, the films were probed with a “Zeiss Axiotech 25H” optical microscope using magnifications between 5 times and 100 times. The micrographs were recorded with a “Hitachi KP-D50” CCD camera.

3. RESULTS AND DISCUSSION

Using XRR to monitor the dependence of the near-surface refractive index profiles on the RH has many advantages: it is non-destructive, the whole profile can be extracted out of one measurement, it gives a resolution in the Ångström regime and one gets averaged information over the whole illuminated sample area.^{24,38,39}

Furthermore, with the chosen film thickness of 50 μm , the highest possible surface sensitivity is achieved due to the limited penetration depth of the X-rays, preventing additional reflection from the glass surface.⁴⁰ Such a reflection from the substrate would be visible by the presence of a second critical angle in the XRR data (as it is found for films with a thickness below 20 μm). The analysis of such data including a reflection from the substrate is more challenging because it would be more difficult to reliably discriminate between enrichment layers near the air interface and enrichment near the interface to the substrate. As a consequence, to emphasize the near-surface composition profile we work with sufficiently thick polymer films.²⁴

The obtained refractive index profiles $\delta(z)$ are easily transferred into composition profiles by applying the rule of three.²⁴ This is possible because P(EHA-stat-20MMA) consists of two components with known refractive indices.

3.1. Composition Profile after 24 h. As we pointed out in the Experimental Section, it is important to have a well-defined starting point before the samples are exposed to higher RHs. Figure 1a shows the XRR curve (symbols) together with the corresponding fit (solid line) measured after the freshly casted sample had been drying for 24 h in a desiccator filled with silica gel which is referred to as the status after the first preparation step. The modulations in the intensity between $q_z = 0.03$ and 0.36 \AA^{-1} already indicate a heterogeneous composition profile in the near-surface region.

In detail, from the refractive index profile in Figure 1b, we extract a weak solubility driven²⁴ enrichment of PMMA with a thickness of 70 Å at the sample surface followed by an enrichment zone of PEHA which converges in an oscillating way to the average composition of the statistical copolymer. This observation is consistent to what is predicted for random multiblock copolymer melts near surfaces.⁴¹ Homogeneous bulk material is observed for $z > 1000 \text{ \AA}$, which corresponds to approximately 9 times the radius of gyration of the copolymer.

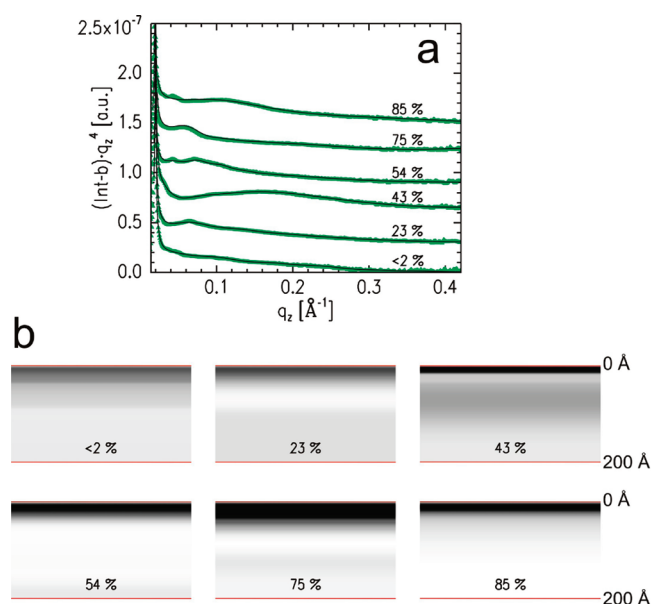


Figure 2. (a) Measured XRR curves (symbols) and corresponding fits (solid lines) for a humidity series of P(EHA-stat-20MMA) in Fresnel-normalized representation. The RH increases from bottom to top as shown by the labels. The data are shifted along the y axis for clarity. (b) Corresponding black and white coded composition profiles. The calculation from the refractive index profiles uses the color code defined in figure 1e.

Figure 1c is a direct conversion of the refractive index profile into a black and white coded representation of the composition profile (for code see Figure 1e). For all investigated samples the main features are observed for $0 < z < 200 \text{ \AA}$. For larger z , we find convergence toward the mean composition 80% PEHA and 20% PMMA in a similar way for all samples. That is why we focus on the near-surface region and show a zoom into the region $0 < z < 200 \text{ \AA}$ (see Figure 1d).

3.2. Humidity Dependence of the Composition Profiles. After the first preparation step which is described in the previous section, the samples are now exposed to a RH controlled environment in which they are stored for additional 24 h. At a total sample age of 48 h, again the near-surface composition profiles are monitored. Figure 2a shows the XRR curves (symbols) for six different RHs and the corresponding fits to the data (solid lines).

The increasing intensity difference between the features at low q_z values and the background level with increasing RH is indicative for an enhanced refractive index contrast in the sample and consequently for increasing heterogeneities along the surface normal within the near-surface region. The extracted composition profiles (see Figure 2b) show this in more detail. Most prominent is the increase in PMMA content at the surface. Except for the composition profile corresponding to a RH of 85%, also the thickness of the PMMA layer increases as a function of time. Simultaneously to these modifications related to PMMA, also the PEHA enriched zone underneath gets more pronounced.

Looking in more detail into the individual behavior, the curve that corresponds to a RH of 2% and thus to a storage time of 48 h under dry conditions has strong similarities to the curve obtained after 24 h (see Figure 1a). As a consequence, the resulting composition profiles are similar. However, there is a small difference in the PMMA content in the vicinity of the surface which is slightly higher for the aged sample (48 h) indicated by

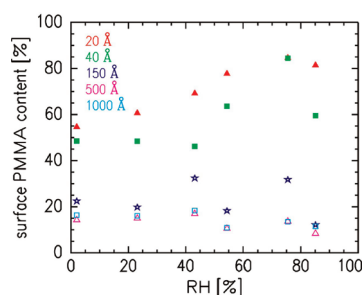


Figure 3. Integrated PMMA content in the near-surface region of P(EHA-stat-20MMA) as a function of the RH. From top to bottom the integration region increases as shown by the labels.

the darker color in the corresponding profile in Figure 2b. This slightly higher PMMA content can be explained by a small amount of residual solvent which is still present after 24 h having the ability to transport the more soluble PMMA with respect to toluene to the surface during evaporation. It has to be noted that the residual solvent cannot be detected because its ratio is in the subpercent regime and it is not enriched in the near-surface region that is accessible with XRR.^{42,43}

In case of the samples exposed to higher RHs, the PMMA enrichment is more pronounced as compared to that in the sample which was completely prepared under dry conditions. An increased amount of evaporated residual solvent cannot be responsible for this behavior because the higher the RH is the less solvent can evaporate. The reason for this is the additional space that is occupied by water vapor in the desiccator for the higher RHs giving rise for a decelerated solvent evaporation. A reduced evaporation of residual solvent leads to a lower near-surface PMMA content. This is consistent with the observations made by Gu and Alexandridis reporting that the drying rate decreases with increasing RH.⁴⁴

As a consequence, the additional PMMA which is detected at the sample surface for higher RHs can only be explained by the enhanced selectivity of the surrounding atmosphere with respect to PMMA. The polarities of the involved components are 0.026 for PEHA⁴⁵ and 0.357 for PMMA⁴⁶ being calculated as the ratio between the polar component of the surface tension and the total surface tension. Under constant temperature, the water vapor content and thus the polarity of the medium in which the samples are placed increases with increasing RH. As a consequence, the more polar PMMA is favored to be adsorbed at the polymer–air interface and the near-surface PMMA concentration increases as a function of RH.

To quantify this phenomenon, we integrate the composition profiles over different depths measured from the surface. We select a range between $z = 0$ and $z = 20, 40, 150, 500,$ and 1000 \AA and plot the corresponding average PMMA content as a function of RH (see figure 3). As the illustration in figure 2b has already suggested qualitatively, the PMMA content in the upper 20 \AA increases monotonically with RH from 55% for dry conditions to 85% for a RH of 75%. Saturation is reached for RHs which are higher than 75%. For broader integration regions the effect of PMMA enrichment gets less pronounced. An averaging of the composition profiles over more than 500 \AA finally leads to a constant PMMA content as a function of RH.

The error of the plotted PMMA concentrations is on the order of the symbol size. It is obtained by slight variations of the refractive index profiles which correspond to the best fit of the

measured data. The fits have been acceptable as long as the respective PMMA concentration does not exceed the height of the symbols in Figure 3.

3.3. Surface Tension As a Function of Relative Humidity.

To relate the installed composition profiles to the resulting mechanical properties, we determine the surface tension of films of P(EHA-stat-20MMA) that are prepared under six different RHs following the presented preparation protocol. We apply the method of Owens and Wendt³⁶ using six different test liquids.

Because the droplets do not equilibrate immediately, it is necessary to record the contact angle as a function of time. We observe a monotonic decay of the contact angle with time which slows down and approaches a limiting value. Because of the onset of evaporation⁴⁷ and dissolution of the polymer, it is not possible to measure until the equilibrium angle θ_f is reached. This observation has already been made by Kano and Akiyama who described the contact angle of organic solvents on P(EHA-co-acrylic acid) as an exponential decay.⁴⁸ Lavi and Marmur introduced one additional parameter when modeling the spreading behavior of partially wetting liquids.⁴⁹

We translate their function to the problem of equilibrating contact angles and use the fit function

$$\theta(t) = \theta_f + (180^\circ - \theta_f) \exp[-k(t - t_0)^m]$$

which is defined for $t \geq t_0$. t_0 is the time when the droplet gets in contact with the substrate. At this point the contact angle is $\theta(t_0) = 180^\circ$. For large times t , $\theta(t)$ converges to θ_f being the equilibrium contact angle. θ_f , k , m , and t_0 are the fitted parameters, where k and m account for the interaction kinetics of the droplet with the adhesive and t_0 is an experimental parameter describing the time delay between the first contact of the droplet with the sample and the start of the measurement. The values for k and m are in the interval $(0, 1.5)$, and t_0 is on the order of seconds.

Figure 4 shows exemplarily the measured contact angles as a function of time with the corresponding fits for P(EHA-stat-20MMA) which was completely prepared under dry conditions. The fitted equilibrated contact angles θ_f are $(23.7 \pm 0.4)^\circ$ for paraffin oil, $(41.4 \pm 1.0)^\circ$ for diiodomethane, $(55.8 \pm 1.3)^\circ$ for ethylene glycol, $(74.9 \pm 0.6)^\circ$ for formamide, $(88.4 \pm 2.6)^\circ$ for glycerol, and $(82.5 \pm 2.3)^\circ$ for water. The errors are the standard deviation of the fitted θ_f of the corresponding curves. For the case of ethylene glycol and formamide, the equilibration times are almost 2 h. Longer measurements have been performed to confirm the fitted θ_f for these two liquids.

The described measurements and the data analysis are carried out for all six samples of the humidity series. As a result, figure 5 shows the corresponding Owens-Wendt plots for the six RHs. In detail, $[1 + \cos(\theta_f)]\gamma/(2\gamma_d^{1/2})$ is plotted as a function of $(\gamma/\gamma_d - 1)^{1/2}$, where γ and γ_d are the total and the dispersive component of the surface tensions of the involved test liquids. By fitting a linear function to these six points for each sample, the surface tensions of P(EHA-stat-20MMA) for the different RHs are obtained: the y-axis intercept is the square root of the dispersive component and the slope is the square root of the polar component of the surface tension. The total surface tension is the sum of both.

The Owens–Wendt plots in Figure 5 already indicate a strong similarity between samples prepared under different RHs. Figure 6 shows from bottom to top the polar component, the dispersive component and the total surface tension as a function of RH. As a result, for all contributions to the surface tension no

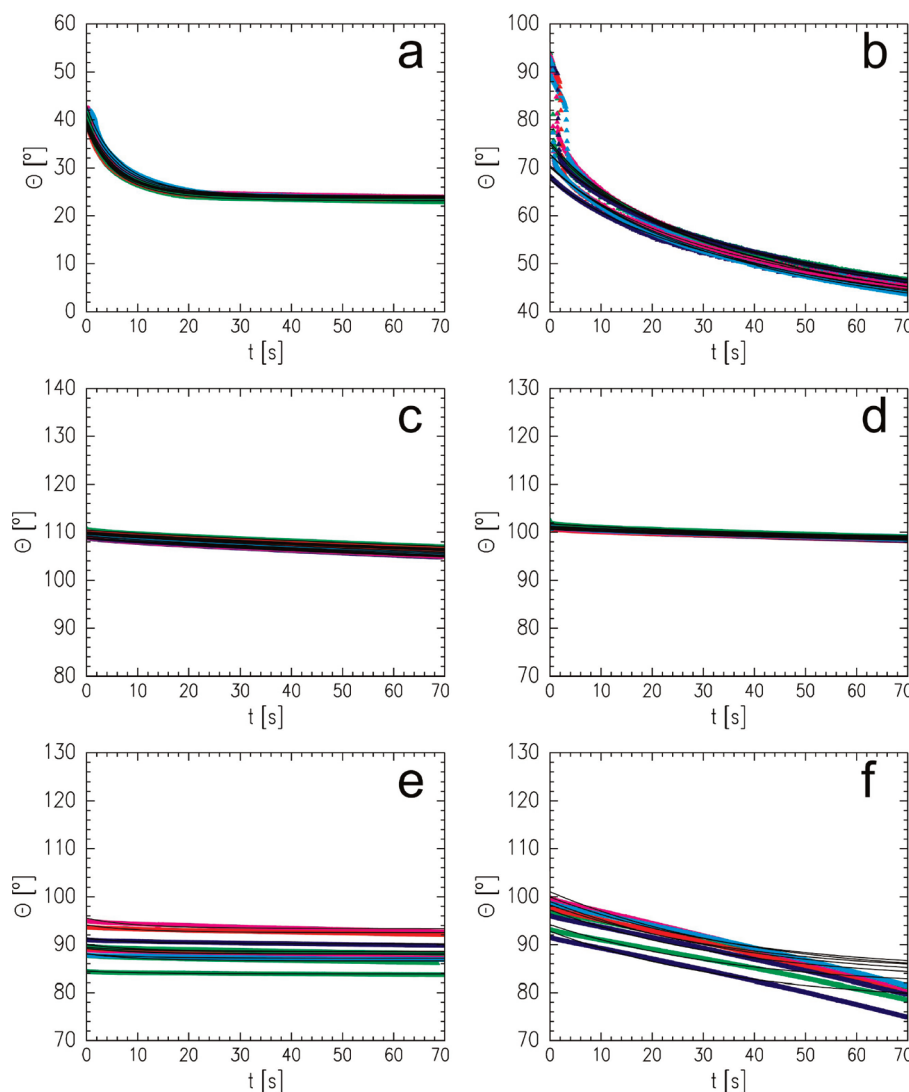


Figure 4. Contact angle θ as a function of time t for six different test liquids on a film of P(EHA-stat-20MMA) prepared under dry conditions. Symbols represent the measured data and the solid lines are the corresponding fits. At least seven curves are measured for each liquid. With increasing polarity, the liquids are (a) paraffin oil, (b) diiodomethane, (c) ethylene glycol, (d) formamide, (e) glycerol, and (f) water.

RH dependence is detected. Irrespective of the RH, we obtain a mean surface tension of $\gamma_p(\text{P(EHA-stat-20MMA)}) = (2.6 \pm 0.6)$ mN/m, $\gamma_d(\text{P(EHA-stat-20MMA)}) = (30.5 \pm 0.8)$ mN/m, and $\gamma(\text{P(EHA-stat-20MMA)}) = (33.1 \pm 0.3)$ mN/m. Literature values of the corresponding homopolymers^{45,46} are $\gamma(\text{PEHA}) = 30.2$ mN/m and $\gamma(\text{PMMA}) = 38.4$ mN/m.

The reason for this result can be found in the installed composition profiles. Although we find a significant enrichment of PMMA at the sample surface, this enrichment layer has only a thickness of less than 70 Å which is in the sub- R_g regime. The interaction between the adhesive and the droplet, however, is determined by the composition profile in the near-surface region up to a certain depth. Figure 3 gives an estimate that the RH correlation is lost for integration depths higher than 500 Å explaining the missing RH dependence of the surface tension.

Observations supporting our findings have already been discussed in literature. Staeger et al., for example, investigated the nanomechanical properties of poly(styrene-*b*-butadiene-*b*-styrene) triblock copolymers with different copolymer formulations and the impact of UV light exposure.⁵⁰ As a result, the

surface stiffness and the adhesive properties were strongly influenced but the surface energy determined with contact angle measurements was unchanged. Similar to that, Falsafi and co-workers found that the surface tension of P(EHA-co-acrylic acid) elastomers was constant as a function of acrylic acid content.⁵¹ In contrast to our work, none of these investigations was able to directly monitor the near-surface composition profile, although it is to be expected that the variation in the respective control parameters changed the surface composition.

3.4. Mechanical Tack Test. The constant surface tension as a function of RH implies that the thermodynamic work of adhesion for a given punch material is identical for all samples in the humidity series.^{52,53} Even so, the adhesive performance does change as a function of RH, which means that this is solely a consequence of the altered near-surface mechanical properties. The effect is demonstrated via probe tack tests, using a punch which is fabricated of either stainless steel or silicon. The tack experiments with the steel punch have been carried out for the same six different RHs as in the presented XRR and contact angle measurements. Additionally, a silicon punch was employed for

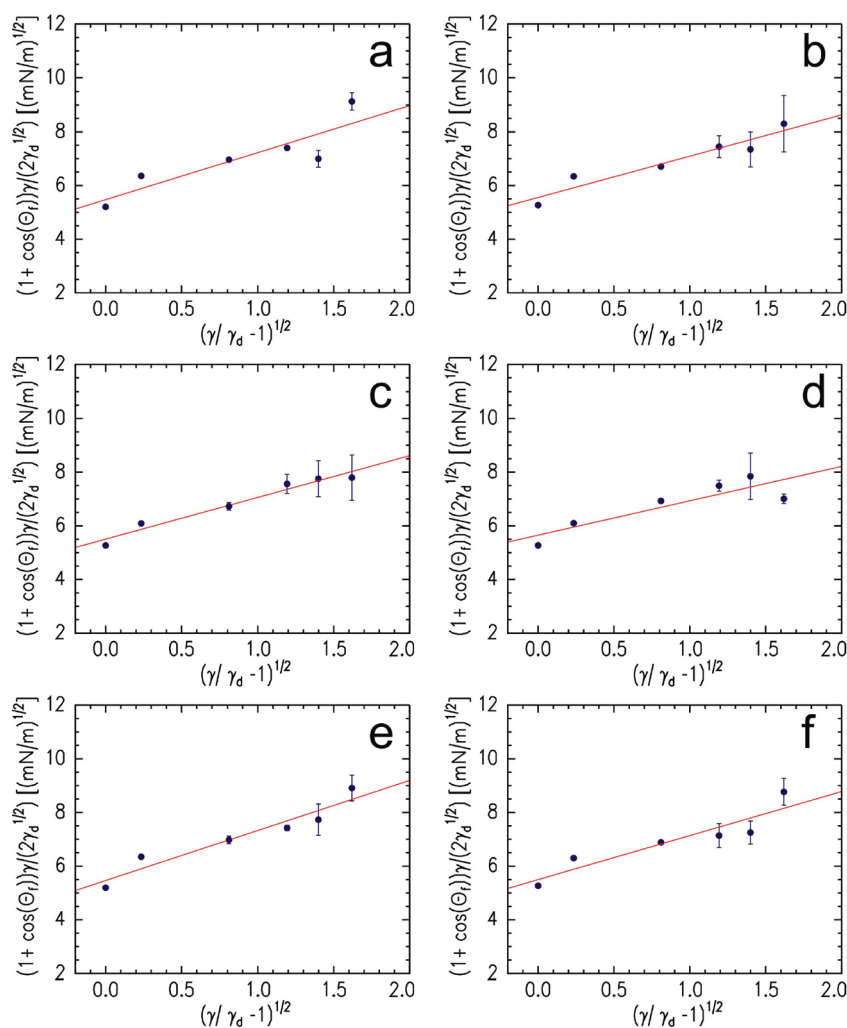


Figure 5. Owens–Wendt plots for P(EHA-stat-20MMA) films prepared under RHs of (a) <math>< 2</math>, (b) 23, (c) 43, (d) 54, (e) 75, and (f) 85%. The symbols represent the mean contact angles θ_f for each test liquid and the solid line is a linear fit to the data.

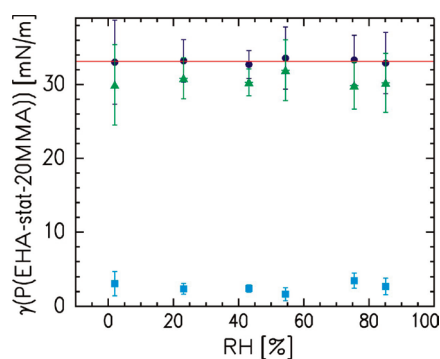


Figure 6. Polar (squares) and dispersive (triangles) components of the total surface tension of P(EHA-stat-20MMA) (circles) as a function of the RH. The solid line marks the mean value of the total surface tension.

measuring the tackiness of samples prepared under dry conditions as well as under a RH of 75%.

Figure 7a exemplarily shows all stress–strain curves for the case of the sample preparation under dry conditions obtained with the steel punch. For all investigated RHs, the shape is rather typical for a non-cross-linked PSA material exhibiting a sharp

stress peak at a strain of around 0.3 which is followed by a plateau region that converges monotonically to 0 starting from a stress value of approximately 0.2 N/mm^2 . Prominent parameters such as the value of the stress maximum and the tack energy are extracted. The latter is equal to the integral of the stress over the strain. For better comparison, all parameters are normalized to the values corresponding to a RH of 75%, for which the best tackiness is achieved. In this case, the absolute values of the stress maximum and the tack energy for the steel punch are $(2.40 \pm 0.34) \text{ N/mm}^2$ and $(65.7 \pm 8.9) \text{ J/m}^2$, respectively. The errors are the standard deviations obtained from at least 8 measurements per sample.

As a result, both the stress maximum and the tack energy increase as a function of RH (see panels c and d in Figure 7). For the tack energies, most of the increase takes place between RHs of 23% and 54%. Because of the higher error bars, such details cannot be derived for the stress maxima. But anyhow, the stress maximum for the sample which is prepared under dry conditions is significantly lower than those for RHs higher than 54%. This behavior is closely related to an increased number of cavities which form during detaching with increasing RH. This is illustrated in Figure 7b showing typical optical images of the punch area probed at the moment when all cavities have evolved. Furthermore, when the punch material is exchanged to silicon

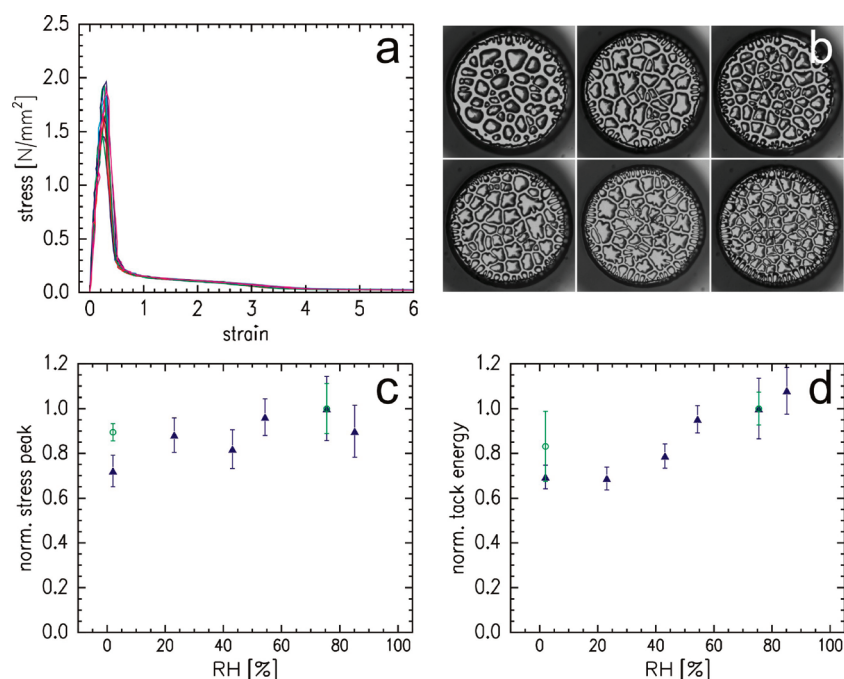


Figure 7. (a) Stress–strain curves for the sample that is prepared under dry conditions. (b) Representative optical images for each sample of the humidity series of the punch area at the moment all cavities have evolved. The RH increases in reading direction. (c) Stress peak as a function of RH normalized to the value at a RH of 75%. Filled triangles correspond to data obtained with a steel punch and open circles are data measured with a silicon punch. (d) Tack energy as a function of RH in analogy to panel c.

instead of steel, the trend remains the same. The amplitudes of the changes in stress maximum and tack energy, however, are reduced by approximately a factor of 2.

The obtained results can only be related to the installed near-surface composition profiles because the bulk material is the same for all investigated samples. Due to the small punch roughness of below 20 Å the main contribution originates from a thin near-surface volume,²⁴ for which the content of the glassy component increases monotonically as a function of RH. In accordance to the tack energy, the steepest increase of PMMA concentration occurs between RHs of 23 and 54% (see Figure 3). For the similar sample system P(EHA-stat-acrylic acid), Lakrouf and co-workers found that the locus of the cavities is also close to the interface.⁵⁴ As a consequence, the observed increased number of cavities for the higher RHs also reflects the higher near-surface PMMA concentration representing the less mobile component. This reduced mobility of the near-surface material limits the cavity growth, preventing the merging of appearing cavities. As a result, for the higher RHs, more cavities with a smaller area are observed. This is also consistent with the findings of Lakrouf and co-workers when comparing the maximum average area of a cavity of pure PEHA with P(EHA-stat-acrylic acid).

Moreover, the increase in the stress maximum and the tack energy with increasing PMMA content can only be a consequence of the altered mechanical properties of the near-surface area. An explanatory approach could be the almost linear relation between the shear storage modulus and the maximum stress, which is demonstrated in ref 54. A direct comparison, however, remains difficult because the bulk rheological properties are not affected by a change in the near-surface composition.

It is not easy to apply existing theories about probe tack tests to our findings because up to now, near-surface material has not been distinguished from bulk material. Anyhow, a promising

ansatz may be the work by Gay and Leibler,⁵⁵ who attributed the appearance of the cavities to interfacial defects arising from the different length scale of the roughness of the punch compared to that of the PSA. They claim that the more rigid the adhesive film is, the more the true contact area is restricted to the summits of the rough surfaces. Since the overall, nominal compressing pressure is 0.32 MPa, it is effectively higher when the true contact area is smaller. Because the XRR measurements show that the surface roughness is almost constant as a function of RH, it can be concluded from the increased near-surface content of the harder component for the higher RHs, that the effective contact pressure increases with increasing RH. As a further consequence, also the stress maximum and the tack energy increase.²⁵

The same trend follows from a work by Shull and Creton in which the stress that is necessary to expand an existing cavity is calculated in terms of pressure.⁵⁶ The higher the Young's modulus of the material, in which the cavity is embedded, the more energy costly its expansion is. So again, under the assumption that the cavities appear close to the interface, a higher RH and, thus, a higher PMMA concentration leads to an increase in tack energy.

It has to be noted, however, that a full theoretical description is still missing, even for homogeneous samples. Nevertheless, to include near-surface composition variations in future theoretical works might be meaningful. Furthermore, experiments about altered mechanical properties close to the interface, possibly via light scattering experiments, could be of interest.

Finally, the decreased amplitude of the effect when exchanging the punch material from steel to silicon can be understood by the interactions of the PSA with the adherent. They affect, for example, the wetting of the punch and the stickiness to the polymer although the surface roughness of the probe is unchanged. For silicon, the ratio between the surface tension of the punch and the polymeric

components is significantly higher than for steel.^{57,58} Therefore, composition variations close to the surface have a bigger impact when steel is chosen as the punch material. In summary, this means that for the tuning of the adhesive performance of a PSA via the RH, also the choice of the material of the adherent plays a significant role.

4. CONCLUSION

For the first time, the near-surface composition profiles of a PSA model system consisting of a two component statistical copolymer (P(EHA-stat-20MMA)) is directly tuned by exposing the samples to atmospheres with the appropriate relative humidity (RH). As a consequence, the tack energy in the extreme cases of almost zero RH and 85% RH differ by approximately 30%.

A suitable preparation protocol has been developed to keep the solvent evaporation speed constant and thus to isolate the influence of the presence of water vapor. XRR is the ideal tool to probe the near-surface molecular composition and gain fundamental understanding of the impact on the macroscopic parameters surface tension and tackiness. As a result, the content of the more polar component (PMMA) close to the sample surface increases monotonically as a function of RH. This effect is most prominent if the mean PMMA content of the upper 20 Å is considered. If the PMMA content is averaged over a thicker near-surface region the effect gets less pronounced until it is fully lost when integrating over more than 500 Å. In other words, with changing the RH of the atmosphere surrounding the PSA film, the near-surface composition is altered up to a depth of 500 Å (measured from the surface).

This observation is related to the mechanical properties. The surface tension, which was determined by the method of Owens and Wendt with six test liquids, does not change as a function of RH. We conclude that the interaction between the test liquids and the samples exceeds the depths for which we detect a pronounced modification of the composition profile.

Mechanical tack tests, however, reveal a clear dependence on the near-surface PMMA concentration within a thin near-surface region having a thickness close to the punch roughness. Both, the stress maximum as well as the tack energy increase monotonically as a function of PMMA content and, thus, as a function of RH. This result reflects the altered near-surface mechanical properties and is further visible by an increased number of cavities with increasing RH. The effect gets less pronounced when a higher surface energy punch material like silicon is chosen.

In summary, this investigation shows the influence of the RH on the molecular structure and the mechanical properties of a PSA model system. For the design of PSAs in special applications, this knowledge could play a key role. In further studies it might be of interest to focus on additional parameters such as temperature, type of solvent, and solvent evaporation rate and determine to what extent they can influence the near-surface composition profile.

AUTHOR INFORMATION

Corresponding Author

*Phone: +498928912451. Fax: +498928912473. E-mail: muellerb@ph.tum.de.

ACKNOWLEDGMENT

We thank B. Russ and P. Böni for their assistance in the XRR experiments and BASF SE for donating the polymer samples.

The financial support by the Deutsche Forschungsgemeinschaft (DFG) in the projects MU 1487/6 and WI 3182/2 is gratefully acknowledged.

REFERENCES

- (1) Müller-Buschbaum, P.; Ittner, T.; Maurer, E.; Köstgens, V.; Petry, W. *Macromol. Mater. Eng.* **2007**, *292*, 825–834.
- (2) Retsos, H.; Gorodyska, G.; Kiriya, A.; Stamm, M.; Creton, C. *Langmuir* **2005**, *21*, 7722–7725.
- (3) Lemieux, M.; Usov, D.; Minko, S.; Stamm, M.; Shulha, H.; Tsukruk, V. V. *Macromolecules* **2003**, *36*, 7244–7255.
- (4) Liu, X.; Ye, Q.; Yu, B.; Liang, Y.; Liu, W.; Zhou, F. *Langmuir* **2010**, *26*, 12377–12382.
- (5) Kessel, S.; Schmidt, S.; Müller, R.; Wischerhoff, E.; Laschewsky, A.; Kutz, J.; Uhlig, K.; Lankenau, A.; Duschl, C.; Fery, A. *Langmuir* **2010**, *26*, 3462–3467.
- (6) Cooperstein, M. A.; Canavan, H. E. *Langmuir* **2010**, *26*, 7695–7707.
- (7) Xie, T.; Xiao, X. *Chem. Mater.* **2008**, *20*, 2866–2868.
- (8) Boyne, J. M.; Millan, E. J.; Webster, I. *Int. J. Adhes. Adhes.* **2001**, *21*, 49–53.
- (9) Chivers, R. A. *Int. J. Adhes. Adhes.* **2001**, *21*, 381–388.
- (10) Chang, T.; Sproat, E. A.; Lai, Y.; Shephard, N. E.; Dillard, D. A. *J. Adhes.* **1997**, *60*, 153–162.
- (11) Moon, S.; Foster, M. D. *Langmuir* **2002**, *18*, 8108–8115.
- (12) Shah, S. S.; Howland, M. C.; Chen, L.; Silangcruz, J.; Verkhoturov, S. V.; Schweikert, E. A.; Parikh, A. N.; Revzin, A. *ACS Appl. Mater. Interfaces* **2009**, *1*, 2592–2601.
- (13) Qu, L.; Dai, L.; Stone, M.; Xia, Z.; Wang, Z. L. *Science* **2008**, *322*, 238–242.
- (14) Hu, S.; Jiang, H.; Xia, Z.; Gao, X. *ACS Appl. Mater. Interfaces* **2010**, *2*, 2570–2578.
- (15) Nadermann, N.; Ning, J.; Jagota, A.; Hui, C. *Langmuir* **2010**, *26*, 15464–15471.
- (16) Feng, X.; Meitl, M. A.; Bowen, M. A.; Huang, Y.; Nuzzo, R. G.; Rogers, J. A. *Langmuir* **2007**, *23*, 12555–12560.
- (17) Cho, K.; Cho, J. H.; Yoon, S.; Park, E. P.; Lee, J.; Han, S.; Lee, K.; Koo, J. *Macromolecules* **2003**, *36*, 2009–2014.
- (18) de Crevoisier, G.; Fabre, P.; Copart, J.; Leibler, L. *Science* **1999**, *285*, 1246–1249.
- (19) Agirre, A.; de las Heras-Alarcón, C.; Wang, T.; Keddie, J. L.; Asua, J. M. *ACS Appl. Mater. Interfaces* **2010**, *2*, 443–451.
- (20) Caquineau, H.; Menut, P.; Deratani, A.; Dupuy, C. *Polym. Eng. Sci.* **2003**, *43*, 798–808.
- (21) Park, M. J.; Balsara, N. P.; Jackson, A. *Macromolecules* **2009**, *42*, 6808–6815.
- (22) Geldhauser, T.; Walheim, S.; Schimmel, Th.; Leiderer, P.; Boneberg, J. *Macromolecules* **2010**, *43*, 1124–1128.
- (23) Klos, J. S.; Romeis, D.; Sommer, J.-U. *J. Chem. Phys.* **2010**, *132*, 024907.
- (24) Diethert, A.; Peykova, Y.; Willenbacher, N.; Müller-Buschbaum, P. *ACS Appl. Mater. Interfaces* **2010**, *2*, 2060–2068.
- (25) Peykova, Y.; Guriyanova, S.; Lebedeva, O. V.; Diethert, A.; Müller-Buschbaum, P.; Willenbacher, N. *Int. J. Adhes. Adhes.* **2010**, *30*, 245–254.
- (26) Zosel, A. *Int. J. Adhes. Adhes.* **1998**, *18*, 265–271.
- (27) Perlich, J.; Memesa, M.; Diethert, A.; Metwalli, E.; Wang, W.; Roth, S. V.; Timmann, A.; Gutmann, J. S.; Müller-Buschbaum, P. *ChemPhysChem* **2009**, *10*, 799–805.
- (28) Müller-Buschbaum, P.; Stamm, M. *Macromolecules* **1998**, *31*, 3686–3692.
- (29) Abul Kashem, M. M.; Perlich, J.; Schulz, L.; Roth, S. V.; Müller-Buschbaum, P. *Macromolecules* **2008**, *41*, 2186–2194.
- (30) Greenspan, L. *J. Res. Natl. Bur. Stand., Sect. A* **1977**, *81*, 89–96.
- (31) Braun, C. *Parrat32*, version 1.6; HMI Berlin: Berlin, 2002.
- (32) Parratt, L. G. *Phys. Rev.* **1954**, *95*, 359–369.

- (33) Bandrup, J.; Immergut, E. H.; Grulke, E. A.; Bloch, D. *Polymer Handbook*, fourth ed.; Wiley-Interscience: Hoboken, NJ, 1999.
- (34) Feidenhans'l, R. *Surf. Sci. Rep.* **1989**, *10*, 105–188.
- (35) Dismukes, E. B. *J. Phys. Chem.* **1959**, *63*, 312–314.
- (36) Owens, D. K.; Wendt, R. C. *J. Appl. Polym. Sci.* **1969**, *13*, 1741–1747.
- (37) Menke, T. J.; Funke, Z.; Maier, R.-D.; Kressler, J. *Macromolecules* **2000**, *33*, 6120–6125.
- (38) Born, M.; Wolf, E. *Principles of Optics*, second ed.; Pergamon Press: Oxford, U.K., 1964.
- (39) James, R. W. *The Optical Principles of the Diffraction of X-rays*; OxBow Press: Woodbridge, CT, 1962.
- (40) Lekner, J. *Theory of Reflection*; Martinus Nijhoff Publishers: Dordrecht, The Netherlands, 1987.
- (41) Donley, J. P.; Fredrickson, G. H. *Macromolecules* **1994**, *27*, 458–467.
- (42) Perlich, J.; Körstgens, V.; Metwalli, E.; Schulz, L.; Georgii, R.; Müller-Buschbaum, P. *Macromolecules* **2009**, *42*, 337–344.
- (43) Zhang, X.; Yager, K. G.; Kang, S.; Fredin, N. J.; Akgun, B.; Satija, S.; Douglas, J. F.; Karim, A.; Jones, R. L. *Macromolecules* **2010**, *43*, 1117–1123.
- (44) Gu, Z.; Alexandridis, P. *Langmuir* **2005**, *21*, 1806–1817.
- (45) Wu, S. *Org. Coat. Plast. Chem.* **1971**, *31*, 27.
- (46) Piglowski, J. M.; Bryjak, M. *Eur. Polym. J.* **1998**, *34*, 1669–1673.
- (47) Erbil, H. Y.; Avci, Y. *Langmuir* **2002**, *18*, 5113–5119.
- (48) Kano, Y.; Akiyama, S. *Polymer* **1993**, *34*, 376–381.
- (49) Lavi, B.; Marmur, A. *Colloids Surf., A: Physicochem. Eng. Asp.* **2004**, *250*, 409–414.
- (50) Staeger, M.; Finot, E.; Brachais, C.-H.; Auguste, S.; Durand, H. *Appl. Surf. Sci.* **2002**, *185*, 231–242.
- (51) Falsafi, A.; Tirrell, M.; Pocius, A. V. *Langmuir* **2000**, *16*, 1816–1824.
- (52) Zosel, A. *Colloid Polym. Sci.* **1985**, *263*, 541–553.
- (53) Israelachvili, J. *Intermolecular & Surface Forces*; Academic Press Inc., 1991.
- (54) Lakrout, H.; Sergot, P.; Creton, C. *J. Adhes.* **1999**, *69*, 307–359.
- (55) Gay, C.; Leibler, L. *Phys. Rev. Lett.* **1999**, *82*, 936–939.
- (56) Shull, K. R.; Creton, C. *J. Polym. Sci., Part B: Polym. Phys.* **2004**, *42*, 4023–4043.
- (57) Mantel, M.; Wightman, J. P. *Surf. Interface Anal.* **1994**, *21*, 595–605.
- (58) Kim, H. J.; Jang, C. E.; Kim, D. E.; Kim, Y. K.; Choa, S. H.; Hong, S. *Tribol. Lett.* **2009**, *34*, 61–73.